Results in Engineering 29 (2026) 108904

Contents lists available at ScienceDirect

Results in Engineering

journal homepage: www.sciencedirect.com/journal/results-in-engineering

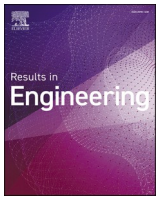

Research paper

Bacterial alginate-based hydrogels reinforced with polysaccharide nanocrystals for water and wastewater decontamination

Daniela Duarte-Serrano [a], Christophe Waterlot [b], Christine Cézard [a], Benjamin Bouvier [c], Cesar Barrientos [d], Italo F. Cuneo [d], Claudia Fuentealba [d], Caroline Hadad [a], Albert Nguyen Van Nhien [a,*]

[a] Laboratoire de Glycochimie et des Agroressources d'Amiens, UR 7378, Université de Picardie Jules Verne - UFR des Sciences, 33 rue Saint Leu, 80039 Amiens Cedex, France
[b] Univ. Lille, Institut Mines-Télécom, Univ. Artois, JUNIA, ULR 4515 – LGCgE, Laboratoire de Génie Civil et géo-Environnement, F-59000 Lille, France
[c] Unité de Génie Enzymatique et Cellulaire, UMR CNRS 7025, Université de Picardie Jules Verne - UFR des Sciences, 33 rue Saint Leu, 80039 Amiens Cedex, France
[d] Escuela de Agronomía, Facultad de Ciencias Agronómicas y de los Alimentos, Pontificia Universidad Católica de Valparaíso, San Francisco s/n La Palma, Quillota, Chile

ARTICLE INFO

Keywords:
Polysaccharide nanocrystals
Adsorption
Isotherm models
Molecular dynamics
In silico modeling

ABSTRACT

The textile industry is a major driver of water pollution, releasing vast amounts of heavy metals, toxic dyes, and organic and inorganic contaminants, which severely harm the environment. Pollution remediation remains a major challenge, highlighting the need for efficient and cost-effective solutions. Biopolymer-based technologies provide a sustainable, efficient, and eco-friendly solution for industrial dye removal. Incorporating nanomaterials can enhance the adsorption capacity of these materials due to their high specific surface area. This study compares the effectiveness of nanomaterials such as cellulose nanocrystals (NCC), chitin nanocrystals (NCChit), and oxidized chitin nanocrystals (NCChit-ox). The results indicate that NCChit-ox is the most effective sorbent, exhibiting the highest Langmuir constant (KL) and a maximum adsorption capacity for methylene blue (MB) of 96.5 mg/g, with a removal efficiency exceeding 92.5 % across all concentrations, as confirmed by molecular modeling. These nanomaterials were incorporated into bacterial alginate-based hydrogels for MB adsorption. The effects of temperature, contact time, pH, and dye concentration were studied. Among the evaluated isotherms, the adsorption experimental data best fit the Langmuir model (R^2 = 0.9547). Kinetic data suggest that the adsorption process follows a second-order mechanism (R^2 = 0.977). The hydrogel demonstrates excellent reusability, maintaining high adsorption efficiency across multiple cycles.

1. Introduction

In 1968, the European Water Charter stated: "There is no life without water" and "Freshwater resources are not inexhaustible. It is essential to preserve, control, and, if possible, increase them." The charter outlines 12 principles that may seem self-evident today. However, in 2016, it was reported that 1.8 billion people still lacked access to safe drinking water, while 2.4 billion lacked access to adequate sanitation. The primary sources of water pollution include: (i) domestic sewage, which accounts for 75–80 % of water pollution; (ii) heavy industrialization which generates waste in the form of toxic chemicals and pollutants; (iii) marine dumping where household garbage continues to be disposed of in oceans by many countries; (iv) oil leaks and spills caused by offshore drilling operations; (v) intensive agriculture, where chemicals in pesticides and fertilizers directly contaminate water due to flooding, heavy rainfall, or excessive irrigation; (vi) global warming due to the rising temperatures and (vii) radioactive waste with accidents still releasing toxic substances into the environment [1–3].

Dyes, extensively used in the pharmaceutical, textile, food, paper, and cosmetics industries, are significant contributors to environmental problems [4]. It is estimated that 7 million tons of various dyes are discharged annually into water bodies by different industries, generating vast amounts of wastewater. This poses a major concern, as most of these dyes are non-biodegradable and carcinogenic, resulting in hazardous consequences for both human health and ecosystems. The adverse effects on aquatic life are particularly severe, primarily due to direct exposure. Indeed, dyes release nitrates and phosphates into the natural environment, increasing the phenomenon of eutrophication,

* Corresponding author.
E-mail address: albert.nguyen-van-nhien@u-picardie.fr (A.N. Van Nhien).

https://doi.org/10.1016/j.rineng.2025.108904
Received 24 June 2025; Received in revised form 24 December 2025; Accepted 25 December 2025
Available online 26 December 2025

defined as excessive phytoplankton growth and resulting in oxygen depletion due to the inhibition of photosynthesis [5]. For humans, exposure to dyes has been linked to health issues ranging from skin irritation to cancer-like diseases [6]. Azo dyes such as congo red (CR) and methylene blue (MB), are among the most widely used in the textile industry and are highly soluble in water. These dyes are known to be carcinogenic and can induce liver and bladder tumors in laboratory animals. Moreover, the reduction of azo dyes, i.e., the cleavage of the dye's azo bond, leads to the formation of mutagenic and carcinogenic aromatic amines, further amplifying their toxicological risks.

There are three main approaches to removing dyes from wastewater: (i) chemical methods, such as precipitation, flotation, electrocoagulation and oxidation. These methods have several disadvantages that limit their suitability for commercial use, including the need for specialized equipment, high energy demands, and extensive use of chemical reagents. By contrast, (ii) biological treatments typically involve the breaking of azo bonds under anaerobic conditions, which generates aromatic amines. These amines are subsequently degraded into small, non-toxic molecules under aerobic conditions. These processes are both cost-effective and environmentally friendly, as they are less harmful than chemical methods. Finally, (iii) physical methods are generally simple procedures which often rely on mass transfer mechanisms. This approach requires minimal use of chemicals and is considered more reliable, as it does not involve living organisms or extensive chemical usage. Physical methods are frequently employed in processes such as membrane filtration and adsorption. The highest removal percentage for physical dye removal techniques ranges from 86.8 % to 99 %, with adsorption being the most effective method. Hydrogels are three-dimensional, network-cross-linked polymers with a highly porous nature and a large number of hydrophilic functional groups (e.g., OH, COOH and SO_3H), enabling them to absorb and retain significant volumes of water. Polysaccharide-based hydrogels [7,8] are excellent candidates for removing heavy metals, dyes, and oil from water due to their high flexibility, tuneable porosity, adjustable surface charge, thermomechanical stability, functionality, fast diffusion, deswelling ability, pH stability, and large surface area [8]. Additionally, the physicochemical properties of these hydrogels can be enhanced by incorporating nanomaterials [9].

Alginate, a linear polysaccharide composed of β-D-mannuronate (M) and its epimer, α-L-guluronate (G), covalently (1,4)-linked in varying sequences, is widely used in the agri-food and pharmaceutical industries. Commercially, alginate is extracted from brown seaweed as soluble sodium alginate but it can also be produced as an extracellular polymer by *Azotobacter vinelandii* and *Pseudomonas* spp [10–12]. It is important to point out that most alginate-based adsorption studies rely on commercial sodium alginate, whereas the present work employs bacterial alginate, which offers the advantage of a controlled and tunable molecular weight. This enables a more rational design of the hydrogel network and a clearer investigation of structure–property–performance relationships. By tailoring bacterial alginate (**BA**) production (i.e., culture conditions during fermentation), it is possible to obtain polysaccharides with reproducible physicochemical characteristics, in terms of molecular weight and M/G distribution. These two parameters are known to affect their properties, resulting in polymers that are of great interest for use in various industrial applications [13,14].

Numerous studies have reported the use of nanocellulose-based materials for water and wastewater treatment, whereas few works focus on nanochitin as an adsorbent or its incorporation into hydrogel matrices for pollutant removal applications [15–19]. In addition, the existing literature often provides limited insight into the surface charge characteristics of polysaccharide nanocrystals and their role in adsorption mechanisms. In the study presented below, we first compared the effectiveness of nanomaterials (cellulose nanocrystals (**NCC**), chitin nanocrystals (**NCChit**) and oxidized nanocrystals (**NCChit-ox**)) to **BA** as adsorbents for the two dyes most commonly found in wastewater: methylene blue (MB) and congo red (CR). The isotherm parameters for MB and CR adsorption on these materials were also evaluated. Molecular dynamics simulations of the nanocrystals in water in the presence of dye molecules have been undertaken in order to gain atom-level information on the interaction of chitin and cellulose with methylene blue (MB) and congo red (CR); to the best of our knowledge, studies combining molecular dynamics simulations with experimental adsorption results to elucidate molecular-scale interactions between polysaccharide nanocrystals, bacterial alginate hydrogels, and dye molecules remain extremely limited.

Finally, the most promising nanomaterials were incorporated into bacterial alginate-based hydrogels to investigate their kinetic and thermodynamic properties, their swelling properties as well as their higher stability during recyclability compared to bacterial alginate without nanomaterials.

2. Results and discussion

2.1. Adsorption on bacterial alginate and polysaccharide-based nanomaterials

Cellulose and chitin, the first and second most abundant natural polysaccharides on Earth, are linear and semi-crystalline polymers composed of highly ordered (crystalline) regions along with some disordered (amorphous) regions in proportions that vary depending on their source [20,21]. Consequently, cellulose nanocrystals (**NCC**) and chitin nanocrystals (**NCChit**) were successfully extracted using traditional acid hydrolysis. **NCC** was produced by hydrolyzing microcrystalline cellulose with H_2SO_4 (64 % weight) at 45 °C for 2 h followed by purification steps [22]. Commercially available chitin was hydrolyzed with aqueous HCl (3 M) for 1.5 h at 90 °C, followed by multiple centrifugation and dialysis steps to achieve neutral pH, as reported in the literature [23]. Subsequent preparation steps for chitin or cellulose nanocrystals preparation included ultrasonication to enhance dispersibility and centrifugation to eliminate aggregates. The resulting dispersions exhibited a white/beige color and remained stable for several months. Additionally, oxidized chitin nanocrystals (**NCChit-ox**) were successfully synthesized via TEMPO-mediated oxidation of **NCChit** in water at pH 10, followed by dialysis. Using chitin nanocrystal instead of bulk chitin to prepare **NCChit-ox** resulted in a high degree of oxidation (DO = 39 %) [24]. Furthermore, lyophilization of the acquired dispersions of **NCC, NCChit** and **NCChit-ox** could prevent bacterial contamination. **NCC, NCChit** and **NCChit-ox** were fully characterized. The data, summarized in the Electronical Supplementary Data (ESI, Table S1) and detailed in the ESI Figures S1-S6, were consistent with the literature and previous work [22,24–26].

Dynamic light scattering (DLS) and zeta (ξ) potential measurements were conducted to determine particle size, colloidal stability, and surface charge. To ensure colloidal stability, nano-sized particles must exhibit an absolute value of the zeta potential greater than 30 mV. The obtained **NCC** exhibited a negative zeta potential of -47.06 ± 0.36 mV, attributed to the sulfate groups introduced during hydrolysis (see ESI, Table S1). These sulphate groups covalently attached to the **NCC** chain create repulsive forces that prevent particle aggregation [27]. By contrast, **NCChit** displayed a positive zeta potential of $+32.44 \pm 3.69$ mV as HCl does not react with hydroxyl groups, suggesting weak electrostatic repulsive forces among **NCChit** (see ESI, Table S1). On the other hand, the **NCChit-ox** surface exhibited a high density of negative charges, evidenced by a zeta potential of -38.93 ± 0.84 mV (see ESI, Table S1), attributed to the high content of sodium carboxylate groups [24].

The effectiveness of polysaccharide-based nanocrystals and bacterial alginate as adsorbents was evaluated based on their nature, size, surface charge, and the type of dye used. Two dyes, methylene blue (MB) and congo red (CR), were studied at various initial concentrations: 0.01, 0.03, 0.05, 0.08 and 0.1 mM for MB and 0.005, 0.008, 0.01, 0.03 and

0.05 mM for CR in milli-Q water with pH 5.5, chosen as a relevant condition since it ensures optimal sorption performance and predominant dye speciation [17]. The removal efficiencies are shown in Fig. 1 and Tables S2 and S3 (see ESI). Fig. 1a clearly illustrates the superior sorption of MB using **NCChit-ox** and **BA**, with a slight decrease in **BA** sorption capacity with rising concentrations that was not observed for **NCChit-ox** (which displayed near-constant capacities of 93–97 %). Interestingly, these two adsorbents were found to be the least effective for CR removal, with **NCChit** emerging as the most suitable sorbent for this dye (Fig. 1b).

The Langmuir and Freundlich constants are summarized in Table 1 (see also Figure S7), and the amount of dye adsorbed at equilibrium (q_e) is listed in Tables S2 and S3 (see ESI). As shown in Table 1, the best sorbent is **NCChit-ox** as it exhibits the highest Langmuir constant (K_L) and the highest maximum adsorption capacity of MB per unit of sorbent (96.5 mg/g). This is a remarkable result, considering that the maximum adsorption of MB on chitin and its chemical derivatives ranges from 6.90 to 69.92 mg/g at room temperature and neutral pH [28–34]. Moreover, the sorption process is spontaneous, as the free Gibbs energy is negative (Table 1). Regarding the Freundlich model, **NCChit-ox** also stands out as the best sorbent. The model has the highest n value, $n = 1.29$, suggesting favorable adsorption intensity as well as a very high Freundlich constant ($K_F = 21.64\ mg^{1-(1/n)}\ L^{1/n}\ /g$) indicating the adsorption capability of **NCChit-ox** (Table 1). Although the efficiency of **BA** is lower, the negative Gibbs free energy demonstrates that the adsorption process is spontaneous and favorable, much like the adsorption observed for **NCChit-ox**.

Furthermore, as shown in Figure S8a (see ESI), the Hall parameter R_L values fall between 0 and 1. According to the study of Hamdaoui and Naffrechoux[35], values of R_L identify the type of isotherm as irreversible ($R_L = 0$), favorable ($0 < R_L < 1$), linear ($R_L = 1$) or unfavorable ($R_L > 1$). Consequently, **NCChit-ox** can be considered as a suitable sorbent for MB adsorption under the experimental conditions. As reported previously, **BA** and **NCChit-ox** are inefficient sorbents for CR. The most appropriate sorbent for CR was **NCChit**. Table 1 shows that the Freundlich isotherm model fits better with the data than the Langmuir model ($R^2 = 0.97$ vs $R^2 = 0.91$, respectively) (see ESI, Figure S9). Considering the values of the Freundlich constants (n and K_F), the adsorption appeared favorable. The parameters of the Langmuir isotherm indicate a strong interaction between **NCChit** and CR (K_L = 53.8 mg/L) and a maximum adsorption of CR slightly higher than 14 mg/g, this adsorption being spontaneous as shown by the negative value of the free Gibbs energy ($\Delta G = -42.5$ KJ/mol). This was also evidenced by the variation of the Hall parameters (see ESI, Figure S8b), ranging from 0.27 to 0.79 for the lowest and the highest concentrations, respectively. In view of these thermodynamic studies, interactions between sorbents (**NCChit** and **NCChit-ox**) and dyes (MB and CR) should differ considerably.

It is important to note that the structure of **NCChit** and **NCChit-ox** remains unchanged after the adsorption of dyes onto the nano-object surface, as shown on the SEM images in Figure S10 (see ESI).

2.2. Molecular dynamics simulations

Molecular dynamics simulations of the nanocrystals in water in the presence of 10 dye molecules have been undertaken in order to gain atom-level information on the interaction of chitin and cellulose with methylene blue (MB) and congo red (CR). A first remark is that for all systems, the nanocrystals remained whole throughout the simulations: no shifting, peeling or dissociation of the glycosidic chains were witnessed. For cellulose, an expected twisting of the nanocrystals was observed because of the competition between inter- and intrachain hydrogen bonding [36,37]. A second remark concerns the reproducibility of the results, as revealed by five independent simulations for each crystal/dye system with differently substituted crystal surfaces and different initial positions of the dye molecules away from the latter. Within the 400-ns timeframe of our simulations, the relative proportion of crystal/dye and dye/dye interactions (discussed below) were found not to depend on these initial conditions. The results presented below are thus averaged over the five independent simulations for each nanocrystal/dye system. MB was found to readily interact with **NCChit, NCChit-ox** and **NCC**. However, MB being a cationic dye, its probability of being adsorbed on an anionic surface is higher (Fig. 2a). On average, there are 7 to 8 MB molecules within a 5 Å distance from the anionic **NCChit-ox** and **NCC** surfaces vs. 4 from the **NCChit** cationic surface. However, this simple picture obscures the fact that dye molecules undergo a competition for binding, either directly on the crystal surface, or with other, already adsorbed dye molecules.

Indeed (Fig. 2c), the stacking of two MB units at the surface does not occur >15 % of the time (as in Fig. 2d, a representative conformation) and the probability of finding a stack of at least three MB units is close to zero, regardless of the considered crystal. Clearly, the interaction of MB molecules with glycosidic units on the crystal surface dominates the inter-MB interaction. Interestingly, when considering anionic surfaces only (**NCChit-ox** and **NCC**), the affinity of MB for chitin seems lower than that for cellulose, which manifests via slightly less direct **NCChit-ox**/chitin contacts and slightly more two-MB stacks on **NCChit-ox**. This could be a consequence of a lesser charged surface and/or of the twisted conformation of cellulose. These results are consistent with the experimental data presented in Fig. 1a: the MB dye removal for **NCC** is lower when compared to **NCChit-ox** and does not increase with the concentration, denoting a saturated monolayer of dyes on the surface of the

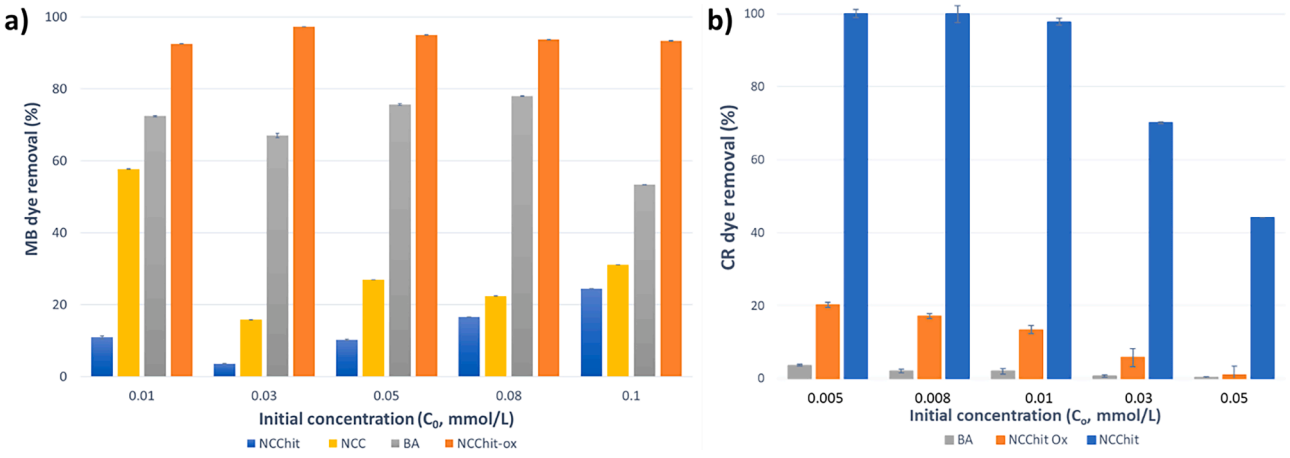

Fig. 1. Effect of initial concentration of a) methylene blue (MB) and b) congo red (CR) on the adsorption capacity of **BA, NCC, NCChit** and **NCChit-ox** at room temperature and neutral pH.

Table 1
Isotherm parameters for MB and CR adsorption on bacterial alginate (**BA**), chitin nanocrystals (**NCChit**), oxidized chitin nanocrystals (**NCChit-ox**) and cellulose nanocrystals (**NCC**).

	Model						
	Langmuir isotherm				Freundlich isotherm		
	q_m[a]	K_L[b]	R^2	ΔG[c]	*n*	K_F[d]	R^2
Methylene blue							
BA	61.39	0.056	0.9520	−23.87	1.09	3.34	0.8411
NCChit	-	-	0.9985	-	0.4133	0.0039	0.9548
NCChit-ox	96.52	0.31	0.8152	−28.06	1.29	21.64	0.9454
NCC	-	-	0.9219	-	0.5966	0.0634	0.9027
Congo red							
BA	-	-	-	-	-	-	-
NCChit	14.11	53.8	0.9081	−42.50	6.03	12.40	0.9709
NCChit-ox	-	-	-	-	-	-	-

[a] (mg/g).
[b] (L/mg).
[c] (KJ/mol.
[d] ($mg^{1-(1/n)}$ $L^{1/n}$ /g).

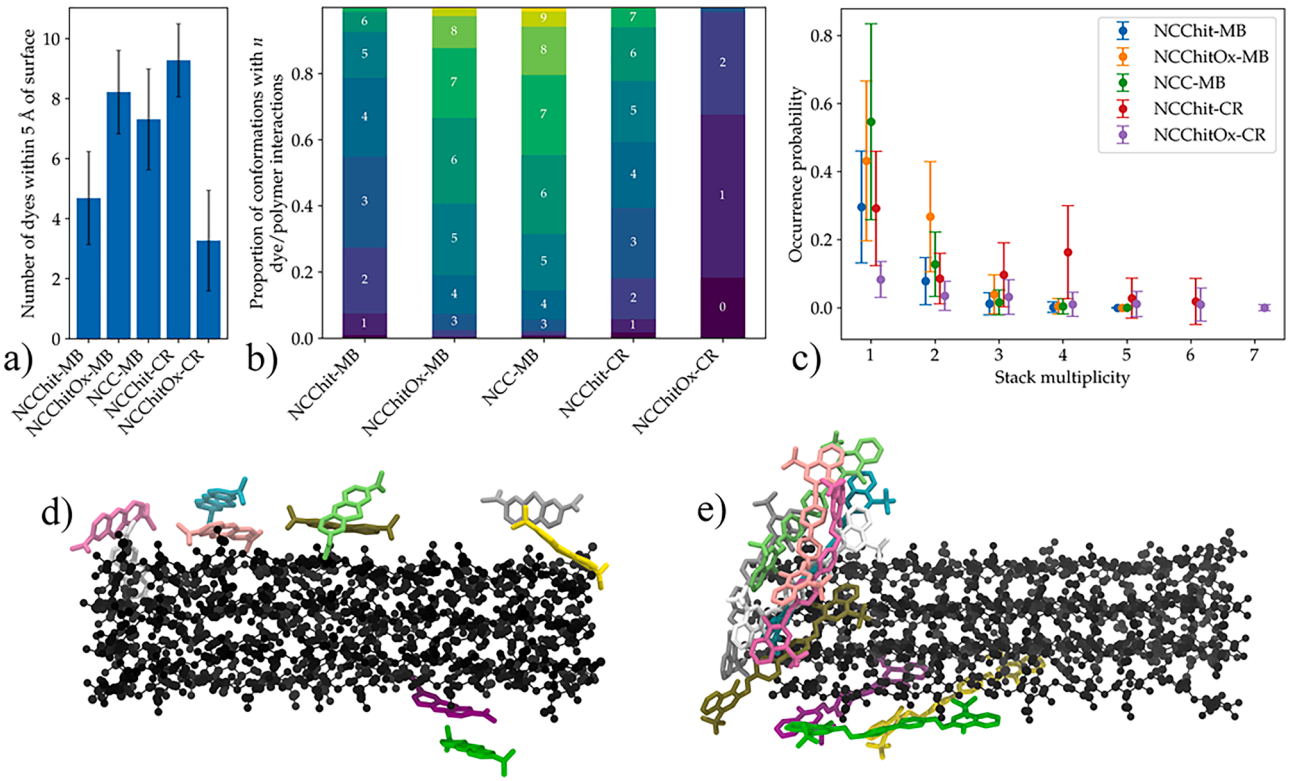

Fig. 2. a) Number of dye molecules within 5 Å of a given nanocrystal. b) Statistics on the number of simultaneous dye/crystal contacts for the systems under study; the number of contacts is given in white within the corresponding bar. c) Statistics on the occurrence of stacks of dyes at the crystal surface for the systems under study. D-e) Conformations representative of the dye-stacking behavior of (d) **NCChit-ox**-MB, where 2-stacks dominate, and (e) **NCChit**-CR, featuring high-count stacks built on top of a limited number of adsorbed CR units (black balls and sticks: chitin; colored sticks: dyes).

crystal. Conversely, the proportion of MB removal is ~100 % regardless of concentration for **NCChit-ox**, indicating a stacking behavior for the dyes. Finally, in line with experiments, **NCChit** is not a good candidate for the removal of MB: chitin/dye interactions do occur to some extent due to the hydrogen-bonding functions on *N*-acetyl-D-glucosamine, but they are severely limited by the expected electrostatic repulsion.

As seen on Figs. 2a–c, interactions of CR with the two kinds of chitin surfaces take place, but CR being an anionic dye, its probability of being adsorbed by a cationic surface is much higher: 3 dyes on average are present within a 5 Å distance from a **NCChit-ox** surface vs. 9 from a **NCChit** surface. This translates into many more direct CR/**NCChit** than CR/**NCChit-ox** contacts (Fig. 2b). Interestingly, 20 % of conformations do not even feature a single CR/**NCChit-ox** contact. Unlike MB, the large size and many aromatic rings of CR tend to favor stacking over electrostatic repulsion between CR moieties; stacking also becomes the only possible interaction once the crystal surface has been covered with bulky CR molecules.

Because of this, stacks of up to 4 CR molecules are frequently observed on **NCChit** (Fig. 2c), and more rarely up to 6; see Fig. 2e for a representative conformation. This correlates with results presented in Fig. 1b where nearly 100 % of dyes are removed by **NCChit** regardless of the concentration. The same stacking behavior applies for **NCChit-ox**; however, due to the small number of direct CR/**NCChit-ox** contacts on which such stacks can be built, their occurrence remains very low

irrespective of the stack size. Again, this trend agrees well with experiments (Fig. 1b), which show a weak removal of CR varying little when the dye concentration is increased.

From our simulations, the dye removal capacities of chitin and cellulose originate from a tradeoff between the relative strengths of dye/crystal adsorption and dye/dye stacking interactions. Dye/crystal interactions are mostly driven by electrostatics (despite possibly mitigating hydrogen bonds). In this regard, **NCChit-ox** in which 40 % of glycosidic units bear a negative charge is highly attractive to cationic dyes such as MB; the covering of the crystal surface by a dye monolayer is thus expected. Comparatively, **NCChit** only features 5 % of positively charged surface moieties and is only mildly attractive to anionic dyes like CR; **NCChit** should thus not be a very efficient CR remover. However, dye/dye stacking interactions can mitigate this picture: whereas the small and rigid MB does not stack very well, the larger and more flexible CR can preserve stacking by better accommodating the electrostatic repulsion between dye molecules. Thus, the experimentally observed near-total removal of dyes at multiple concentrations has different origins: for **NCChit-ox**/MB, it is linked to a monolayer of MB densely covering the chitin surface, while for **NCChit**/CR it is due to the progressive stacking of multiple CR units on a rather sparse first layer.

Importantly, the dye/crystal vs. dye/dye tradeoff is not symmetrical, since stacks cannot be built unless a first interaction layer exists (which explains the weak CR removing properties of **NCChit-ox**); a careful tuning of dye/crystal interactions is thus necessary in all cases.

2.3. Methylene blue adsorption in BA-based hydrogels

Because of the very good dispersibility of MB-nanocrystals in water, we attempted to mix MB, **BA**, and polysaccharide-based nanomaterials in order to obtain hydrogels upon $CaCl_2$ addition. Indeed, hydrogels can be easily removed from water and therefore reused. Before exploring the thermodynamic and kinetic aspects of the retention of MB by **BA**-based hydrogels, their removal efficiencies were studied. The results are summarized in Fig. 3A and Table S4 (see ESI). These results clearly demonstrate the ability of **BA** to adsorb MB. Surprisingly, they highlight lower retention efficiency when **BA** was mixed with nanocrystals, reflecting potential interactions between **BA** and nanocrystals. The most relevant system was the **BA** + **NCChit-ox** hydrogel which achieved dye retentions ranging from 33.4 to 99.7 %, depending on the concentration. The Langmuir and Freundlich models are summarized in Fig. 4 and the amount of dye adsorbed at equilibrium (q_e) is listed in Table S4 (see ESI). Despite the complexity of the sorbents, the determination coefficients for these two models ranged from 0.76 to 0.97 and the Langmuir model fitted well with the data set. This indicates that the sorption of MB on **BA** and **BA** + **NCChit-ox** hydrogels aligns with the assumptions of the Langmuir model. Under the experimental conditions and with this sorbent, the maximum adsorption of MB ($q_m = 6.08$ mg/g) was three times higher than that achieved using **BA** alone ($q_m = 2.28$ mg/g).

In spite of the low value of the Langmuir constant, we assume a spontaneous sorption since it was possible to remove the **BA** + **NCChit-ox** / MB hydrogels from the solution as shown in Fig. 3B On the other hand, the Freundlich model indicated favorable adsorption intensity ($n = 1.20$) but with a very low Freundlich constant ($K_F = 1.11$ $mg^{1-(1/n)}$ $L^{1/n}$/g), casting doubt on the presence of a monomolecular layer of MB on the surface of the **BA** + **NCChit-ox** hydrogels (Table 2).

Fig. 5 presents the FTIR spectra of bacterial alginate (**BA**), oxidized chitin nanocrystals (**NCChit-ox**), methylene blue (MB), and the hydrogels before and after MB adsorption (**BA** hydrogel and **BA**/MB hydrogel, **BA** + **NCChit-ox** hydrogel and **BA** + **NCChit-ox** / MB hydrogel). The spectrum of bacterial alginate (**BA**) exhibits two intense bands at 1611 cm^{-1} (asymmetric) and 1394 cm^{-1} (symmetric), which are characteristic of the stretching vibrations of carboxylate groups ($-COO^-$) in alginate.

Additionally, the characteristic bands of C—O vibrations, typical of polysaccharides, are observed between 1000 and 1200 cm^{-1}. A broad band is also present between 3200 and 3600 cm^{-1}, corresponding to the stretching vibrations of O—H bonds, which are often associated with moisture or hydroxyl groups in polysaccharides such as alginate. In the hydrogel spectra, a broadening of the O—H bands (3200–3600 cm^{-1}) is observed, indicating enhanced hydrogen bonding interactions between molecules in the gel network. Furthermore, a slight shift of the band at 1394 cm^{-1} to higher wavenumbers (≈ 1425 cm^{-1}) confirms the presence of strong interactions between the molecules within the hydrogel network. The oxidized chitin nanocrystals (**NCChit-ox**), present in small quantities (4 mg compared to 16 mg for **BA**), produce signals that are too weak relative to the abundant groups in **BA** (carboxylates, hydroxyls).

These signals are therefore masked by the more intense bands of the BA hydrogel, implying that the spectrum of the **BA** + **NCChit-ox** hydrogel is nearly identical to that of the **BA** hydrogel. Finally, the physical adsorption of methylene blue (MB) within the hydrogels does not alter the chemical nature of either MB or the hydrogel network. Consequently, the characteristic bands of both components remain unchanged in the infrared spectrum [38,39].

It is well established that contact time is a key factor influencing the adsorption rate in the sorbent-solute adsorption process. The influence of contact time on the removal of MB using **BA** and **BA** + **NCChit-ox** hydrogels is presented in Fig. 6A. Based on these results and the Equations 14 and 15, the pseudo-first order (PFO) model (Fig. 6B) and the

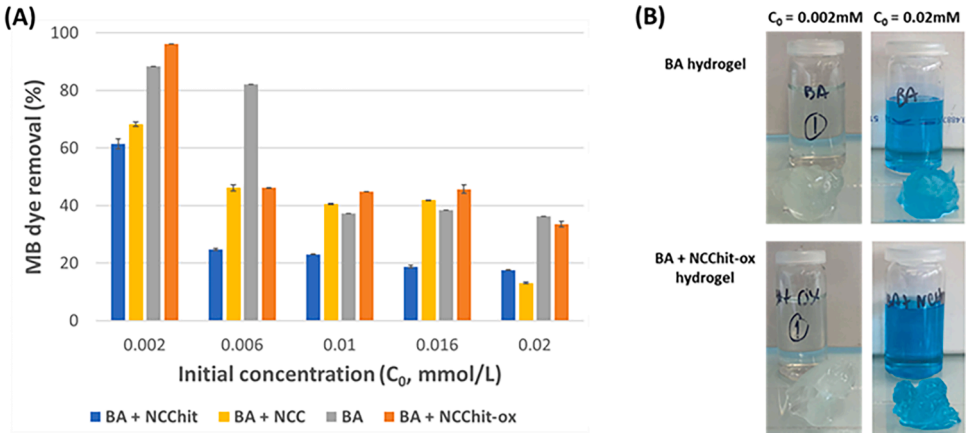

Fig. 3. (A) Effect of initial concentrations of methylene blue (MB) on the adsorption capacity of bacterial alginate (**BA**), bacterial alginate with cellulose nanocrystals (**BA** + **NCC**), bacterial alginate with chitin nanocrystals (**BA** + **NCChit**) bacterial alginate with oxidized chitin nanocrystals (**BA** + **NCChit-ox**) hydrogels at room temperature and neutral pH. (B) Images of bacterial alginate (**BA**) and bacterial alginate with oxidized chitin nanocrystals (**BA** + **NCChit-ox**) hydrogels after adsorption of MB at initial concentrations (C_0) of 0.002 mM and 0.02 mM.

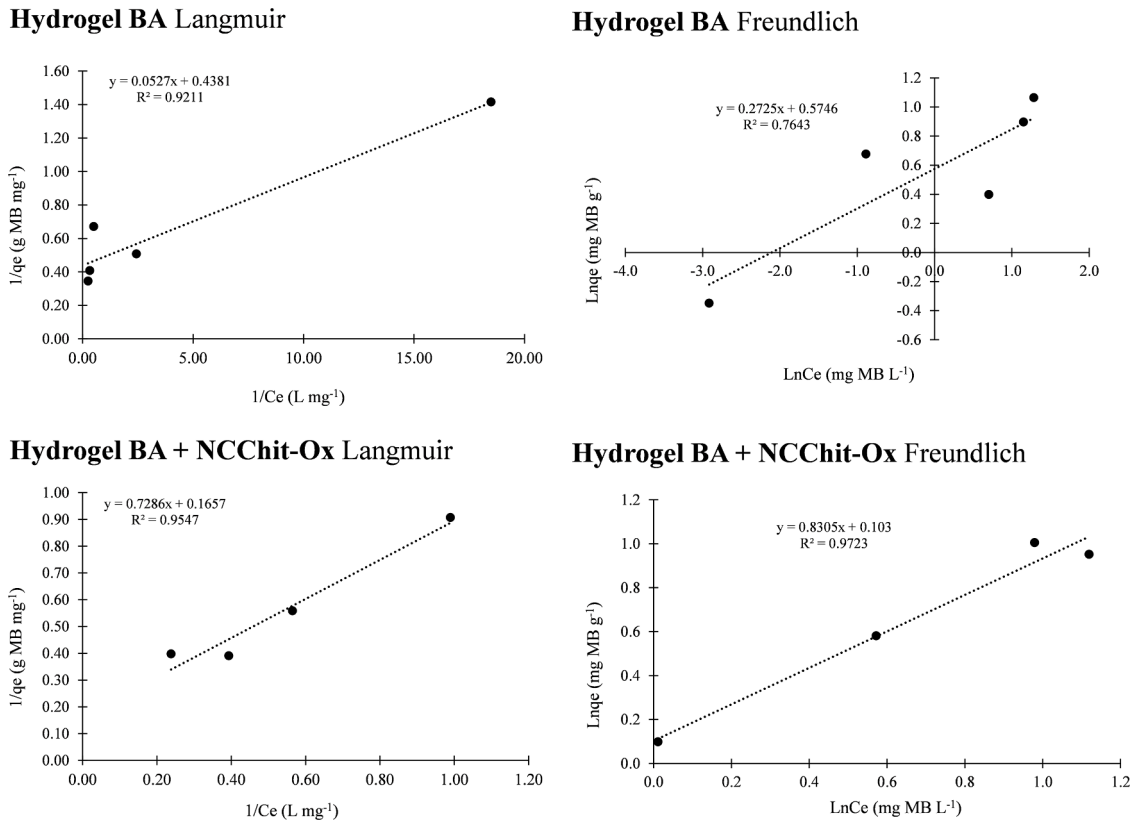

Fig. 4. Isotherm parameters for MB adsorption on bacterial alginate (**BA**) and bacterial alginate with oxidized chitin nanocrystals (**BA + NCChit-ox**) hydrogels: Langmuir and Freundlich models.

Table 2
Isotherm parameters for MB adsorption on bacterial alginate (**BA**) and bacterial alginate with oxidized chitin nanocrystals (**BA+ NCChit-ox**) hydrogels.

	Model					
	Langmuir isotherm			Freundlich isotherm		
Hydrogels	q_m [A]	K_L [b]	R^2	*n*	K_F [c]	R^2
BA	2.28	8.31	0.9211	3.67	1.78	0.7643
BA + NCChit-ox	6.03	0.227	0.9547	1.20	1.11	0.9723

[a] (mg/g).
[b] (L/mg).
[c] ($mg^{1-(1/n)}$ $L^{1/n}$ /g).

pseudo-second order (PSO) model (Fig. 6C) were plotted. From these graphs, the experimental data fit well with the PFO kinetic model for both **BA** and **BA + NCChit-ox** hydrogel sorbents, for which the highest correlation coefficients were obtained (Table 2). As shown in Table 3, the calculated equilibrium adsorption capacity ($q_{e,cal}$) is consistent with the experimental data ($q_{e,exp}$) for both sorbents and the absorption rates are 0.0295 for BA and 0.0030 g/mg min for **BA + NCChit-ox** hydrogels, respectively. Compared to the PFO adsorption model, the values of ($q_{e,cal}$) and R^2 were slightly lower – particularly for **BA**, for which the agreement between $q_{e,cal}$ and $q_{e,exp}$ was not ideal (Table 3).

The thermodynamic studies were conducted using two hydrogels. The corresponding results calculated using Equations 16 to 18, are reported in Table 3. The negative ΔG° values between 298 and 328 K indicate that the sorption of MB on **BA** and **BA + NCChit-ox** hydrogels was spontaneous. The negative enthalpy values (ΔH°) confirm that the sorption was an exothermic process. Therefore, according to Van't Hoff's law, the equilibrium constant will decrease as the temperature increases, meaning that adsorption will be unfavorable. As shown in Table 3, the entropy (ΔS°) values were also negative for both sorbents, indicating an increase in molecular order at the solid/solution interface during the MB dye adsorption.

In addition to the Langmuir and Freundlich isotherm models, the Dubinin-Radushkevich isotherm model (Eqs. 11 and 13) was also used to compute the free energy of adsorption and identify the physical or chemical nature of the sorption process. The free energy of the transfer of one mole of MB to the surface of **BA** and **BA + NCChit-ox** hydrogels was 8.08 kJ/mol and 12.38 kJ/mol, respectively. These values fall within the 8–16 kJ/mol range, denoting a predominantly chemical sorption most likely due to charge-charge interactions [40,41].

The swelling kinetics and capacity of the **BA**-hydrogel were analyzed and compared with those of the **BA + NCChit-ox** hydrogel to evaluate the impact of the nanomaterials' presence. To achieve this, the hydrogels were immersed in water for specific time intervals (5 min, 10 min, 0.5 h, 1.5 h, 6 h, 1 day, 2 days and 3 days). Afterward, the unabsorbed water was removed by filtration, and the swollen gel was weighed. BA and "**BA + NCChit-ox**" hydrogels reached equilibrium after 30 and 90 min of swelling, respectively. The results present Table S5 (see ESI) indicate that the addition of **NCChit-ox** to the **BA** hydrogel leads to a slight increase in the degree of swelling (from 292.32 % to 300.18 %) and water content (from 196.16 % to 200.09 %).

This improvement suggests that the incorporation of nanomaterials can positively influence the swelling properties of hydrogels [42]. Indeed, Siqueira et al.[43]. demonstrated that the addition of cellulose nanocrystals to alginate hydrogels influences their swelling degree, primarily due to their unique structural and chemical properties. Cellulose nanocrystals possess a high number of hydrophilic functional groups (mainly hydroxyl groups) on their surface, which attract and retain water, thereby increasing the swelling capability of the hydrogels.

2.4. Desorption study and recycling

Fig. 7 illustrates the reusability of the hydrogel for the adsorption of

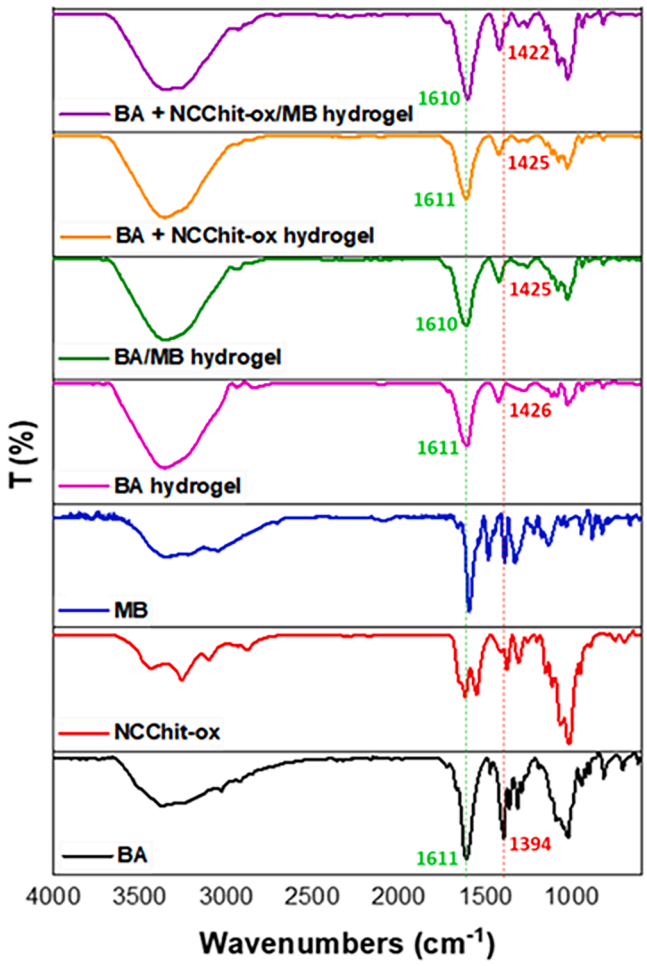

Fig. 5. FTIR of bacterial alginate (**BA**), oxidized chitin nanocrystals (**NCChit-ox**), methylene blue (MB), and the hydrogels before and after MB adsorption (**BA** hydrogel and **BA**/MB hydrogel, **BA** + **NCChit-ox** hydrogel, and **BA** + **NCChit-ox** / MB hydrogel).

MB at an initial concentration of 0.002 mM, over three consecutive cycles. During the first reuse cycle, the adsorption efficiency remains above 90 %, indicating minimal loss of performance. However, a gradual decrease is observed in the second and third cycles, with R % remaining above 80 % but slightly dropping. This decline may be attributed to the partial saturation of the adsorption sites or minor structural changes in the hydrogel after repeated use. Nevertheless, the hydrogel demonstrates excellent reusability, maintaining high adsorption efficiency over multiple cycles, which highlights its potential for sustainable applications in dye removal from aqueous solutions. It is important to note that the recycling of the hydrogel containing only BA did not produce good results. Indeed, after the second recycling, the hydrogel degraded and collapsed, leading to inconsistent and non-reproducible results. This confirms that nanocrystals enhance the mechanical properties of the hydrogel.

3. Experimental

3.1. Materials

Commercially available chitin derived from shrimp shells, microcrystalline cellulose (MCC), 2,2,6,6-tetramethylpiperidine-1-oxyl (TEMPO), sodium bromide, sodium hypochlorite, methylene blue (MB) and Congo red (CR) were purchased from Sigma–Aldrich (Sigma–Aldrich, Steinheim, Germany). All solvents and reagents used in this study were of analytical grade and were purchased from Merck (Darmstadt, Germany).

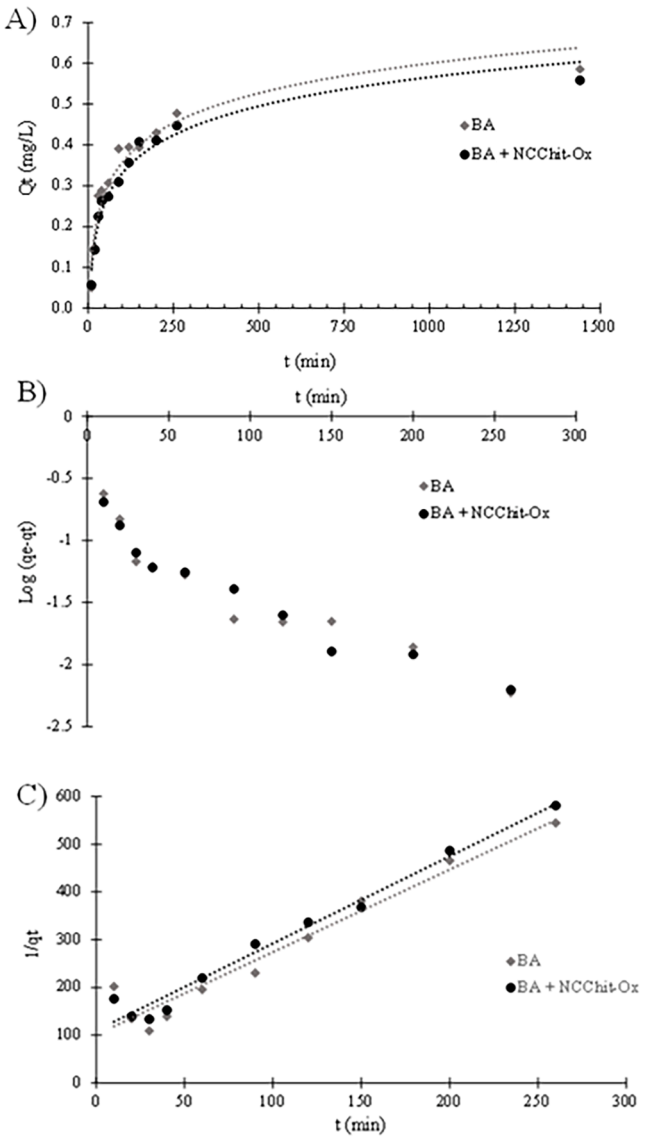

Fig. 6. Adsorption kinetics for MB dye onto **BA** (grey points and lines) and **BA** + **NCChit-ox** hydrogels (black points and lines) at room temperature and neutral pH: A) adsorption capacity vs. time; B) pseudo-first-order kinetic models; C) pseudo-second order kinetic models.

3.2. Instrumental analyses

The infrared spectra were recorded using a Fourier transform infrared (FTIR) spectrometer (IRaffinity-1S, Shimadzu) equipped with an ATR accessory featuring a germanium prism (MIRacle 10, Shimadzu). Spectra were collected in the range of 4000–700 cm^{-1}. X-Ray powder diffraction (XRD) patterns were acquired using a Bruker D8 Endeavor diffractometer equipped with a Cu anti-cathode (Kα radiation, operating at 40 kV–40 mA). Crystallinity indexes (CrI) were calculated from the X-ray diffractograms using Equation 1 (Eq. 1: CrI = ((Intensity max - Intensity amorph)/Intensity max)*100) [24]. The microstructure of the nanocrystals was examined using scanning electron microscopy (SEM) with an FEI Co. scanning electron microscope (USA). All these analyses were conducted following the methodology of Huet et al.[44]. as detailed in the electronic supplementary information (ESI). Zeta potential (ZP) and particle size measurements were performed using

Table 3
Kinetic and thermodynamics parameters for MB adsorption on **BA** and **BA + NCChit-ox** hydrogels.

			BA hydrogel	BA + NCChit-ox
Kinetic parameters	*Pseudo-first-order*	$q_{e,cal}$ [*,a]	0.486	0.579
		K_1 [b]	0.005	0.006
		R^2	0.877	0.931
	Pseudo-second-order	$q_{e,cal}$ [*,c]	0.579	0.548
		K_2 [d]	0.030	0.003
		R^2	0.943	0.977
Thermodynamic parameters	*Enthalpy*	**ΔH° (kJ/mol)**	−30.64 ± 0.88	−15.00 ± 0.69
	Entropy	**ΔS° (J/mol)**	−56.69 ± 2.85	−4.96 ± 2.27
	Gibbs energy	**ΔG° (kJ/mol)**		
		298 K	−13.83 ± 0.03	−13.37 ± 0.00
		308 K	−12.97 ± 0.00	−13.45 ± 0.00
		318 K	−12.71 ± 0.03	−14.06 ± 0.01
		328 K	−13.50 ± 0.02	−12.95 ± 0.07

[*] $q_{e,exp}$ = 0.5854 mg/g.
[a] (mg/g).
[b] (min^{-1}).
[c] (mg/g).
[d] (g/mg min).

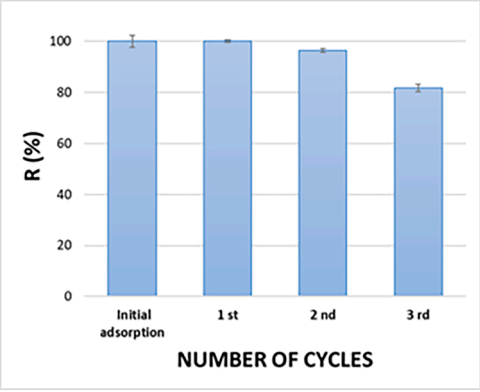

Fig. 7. Removal efficiencies for MB (C_0 = 0.002 mM) with **BA + NCChit-ox** hydrogel as adsorbents after consecutive reuse cycles. Note: After each cycle, hydrogels were simply washed with water.

dynamic light scattering (DLS) with a Zetasizer Nano PRO (Malvern Instruments) operated with a 633 nm laser and at two scattering angles of 173 and 13° respectively. The samples were equilibrated at 25 °C for 120 s prior to measurement to avoid convection artifacts. ZP measurements were carried out in single-use disposable folded capillary cells (model DTS 1070) provided by Malvern Instruments. All samples were prepared at a concentration of 1 mg/mL in Milli-Q water (18.3 MΩ/cm). The degree of oxidation (DO) of oxidized chitin nanocrystals was determined by conductometric titration. For this purpose, 30 mg of oxidized nanocrystals were dispersed in 15 mL of 0.01 M HCl solution using an ultrasonic bath for 30 min and conductivity changes were recorded using a conductometer (4510, Jenway). The titration curve was then used to calculate the degree of oxidation with Equation 2 [45] (Eq. 2: DO (%)=(202*(V2-V1)*c)/(m-36*(V2-V1)*c) x 100, where 202 is the molecular weight of *N*-acetylglucosamine unit (g/mol), 36 is the difference between the *N*-acetylglucosamine unit and the sodium salt of an *N*-acetylglucosamine acid moiety (g/mol), c is the NaOH concentration (mol/L), m is the sample mass (g), and V1 and V2 are the volumes of NaOH (L) corresponding to the first inflection point and the equivalence point on the titration curve, respectively).

3.3. Synthesis of bacterial alginate (BA)

Bacterial strains of *Azotobacter vinelandii* ATCC 9046 (American Type Culture Collection, Manassas, VA, USA) were cultivated in a medium under atmospheric nitrogen fixation conditions using sucrose as the carbon source. The fermentation and the alginate recovery were carried out following the method of Padilla-Córdova et al.[46]. The final solid product had a molecular weight (MW) of 453 ± 42 kDa [47]. The bacterial alginate (BA) was stored in a dried state until it was rehydrated for further analyses.

3.4. Synthesis of chitin nanocrystals (NCChit)

Chitin derived from shrimp shells (4.0 g) was added to 80 mL of 3 mol/L HCl and stirred under reflux at 100 °C for 90 min. The pH was neutralized by washing the precipitate through centrifugation at 9500 rpm for 20 min, repeated five times with Milli-Q water (18.3 MΩ·cm^{-1}). After each centrifugation step, the supernatant was discarded. The resulting precipitate was resuspended in MQ water and subjected to dialysis using dialysis membranes (Average flat width 35 mm (1.4 in), MWCO 12 000 Da) for three days. The dialysis water was replaced three times per day with fresh Milli-Q water. Following dialysis, the suspension was ultrasonicated for 10 min (1 s on/1 s off cycle; 25 % amplitude) using a Vibra-cell ultrasonic processor (Vibra-cell 75,022, 130 W, 20 kHz, sonic tip diameter 13 mm). The suspension was then centrifuged sequentially at 7500, 8500 and 9500 rpm. After each step, the precipitate was removed, and the final suspension containing chitin nanocrystals (NCChit) was obtained and the precipitate was removed after each step. The yield of nanocrystals (white solid, 46 %) was determined by lyophilizing the final acquired suspension and calculating the weight difference between the starting material (commercial chitin) and the final product (NCChit).

3.5. Synthesis of oxidized chitin nanocrystals (NCChit-ox)

A TEMPO-mediated oxidation reaction was performed using 3 g of chitin nanocrystals (**NCChit**) dispersed in 150 mL of water, with the addition of 0.3 g of sodium bromide (NaBr), 0.048 g of TEMPO and 15 mL of sodium hypochlorite (NaClO). The reaction was carried out at pH 10, maintained by using an automatic titrator through the controlled addition of 0.1 M NaOH, under constant stirring at room temperature (RT) overnight. After the reaction, the suspension was subjected to dialysis (MWCO: 12 kDa) for 3–4 days to remove residual reagents and by-products. The yield of oxidized chitin nanocrystals (**NCChit-ox**) was determined as 27 % (white solid) by lyophilizing the final suspension and calculating the weight difference between the starting material (**NCChit**) and the final product (**NCChit-ox**).

3.6. Synthesis of cellulose nanocrystals (NCC)

Microcrystalline cellulose (MCC, 10 g) was suspended in Milli-Q water (45 mL) and cooled to 0 °C. H_2SO_4 (43 mL) was added dropwise at 0 °C under constant stirring until the desired acid concentration (64 % w/w) was achieved [48,49]. The mixture was then heated to 45 °C and stirred for 2 h. Hydrolysis was stopped by diluting the mixture ten-fold with water. The suspension was allowed to settle overnight, after which the supernatant (water and acid) was removed and replaced with fresh Milli-Q water. This washing step was repeated twice. Then, the resulting suspension was transferred into dialysis membranes (12 kD cut-off) and dialyzed against MilliQ water for 3 days, until a neutral pH was achieved outside the membrane. The suspension was centrifuged at 9000 rpm, dispersed by sonication, and the supernatants were collected. This centrifugation-sonication cycle was repeated until the supernatants

were no longer turbid. The yield of cellulose nanocrystals (**NCC**, white solid) was determined as 28 % by lyophilizing the final suspension and calculating the weight difference between the starting material (MCC) and the final product (**NCC**).

3.7. Hydrogel formation

Sixteen mg of bacterial alginate (**BA**) and 4 mg of nanomaterials (**NCC, NCChit** or **NCChit-ox**) were added to 1 mL of water and dispersed by sonication for 1 h (sonic bath). A solution of $CaCl_2$ (4 mL, 2 % w/v) was then added to the as-prepared sample and the reaction was allowed to proceed for 1 h without magnetic stirring to form the hydrogel [13,47,50].

3.8. Swelling properties

Three replicas of each dried alginate-based hydrogel (**BA** and **BA + NCChit-ox**) were immersed in deionized water at room temperature for 3 d to achieve equilibrium swelling. The degree of swelling was measured at various end times: 5 min, 10 min, 0.5 h, 1.5 h, 6 h, 1 d, 2 d and 3 d The degree of swelling was calculated using the Equation 3 (Eq.3: Degree of swelling = [(Wet weight – Dry weight) / Dry weight] ×100 %).

The water content of the hydrogels was determined after achieving equilibrium swelling using the Equation 4 (Eq. 4: Water content = (Wet weight / Dry weight) ×100 %).

3.9. Dye adsorption on bacterial alginate (BA) and polysaccharide-based nanomaterials (NCC, NCChit and NCChit-ox) and their hydrogels

Ten mg of **BA, NCC, NCChit** or **NCChit-ox** were added to 12.5 mL of dye solution at initial concentrations (C_0) of 0.01, 0.03, 0.05, 0.08 and 0.1 mM for methylene blue (MB) and 0.005, 0.008, 0.01, 0.03 and 0.05 mM for Congo red (CR). The mixtures were vigorously stirred for 5 min at room temperature. The dispersions were then centrifuged for 20 min at 12 000 rpm, and the supernatants were analyzed by UV–Vis spectroscopy to indirectly determine the amount of dye adsorbed by the BA or polysaccharide-based nanomaterials. The UV–Vis spectrophotometer results showed maximum absorbance peaks at 660 nm and 497 nm for MB and CR, respectively. Standard solutions of MB and CR at various concentrations were prepared and analyzed at their corresponding wavelengths to generate calibration curves. The standard curves, constructed by plotting absorbance versus concentration, yielded correlation coefficients (R^2) of 0.9949 for MB and 0.9989 for CR. (see ESI, Figures S11). The dye concentrations after adsorption (C_e) were measured in triplicate using the UV–VIS spectrophotometer.

The removal efficiencies (R) of MB or CR were calculated using Equation 5 (Eq. 5: $R = ((C_0 - C_e) / C_e) \times 100$).

The amount of adsorbate adsorbed at equilibrium (q_e) was calculated using Equation 6 (Eq. 6: $q_e = ((C_0 - C_e) / m) \times V$, where q_e represents the equilibrium mass of adsorbed substance per unit mass of adsorbent (mg/g), C_0 is the initial dye concentration (mg/L), C_e is the equilibrium dye concentration (mg/L), V is the volume of solution (mL) and m is the adsorbent mass (g)). Hydrogels were prepared following the procedure described in "Hydrogel formation". Specifically, 16 mg of BA combined with 4 mg of nanomaterials (**NCC, NCChit**, or **NCChit-ox**) or 20 mg of **BA** alone were added to 1 mL of MB solution at concentrations of 0.03, 0.08, and 0.1 mM. The mixture was sonicated in an ultrasound bath for 1 h at RT. Subsequently, 4 mL of a 2 % $CaCl_2$ solution was added to the dispersion and left unstirred for 24 h to allow hydrogel formation. The initial concentrations (C_0) of MB were 0.02, 0.016 and 0.01, 0.006 and 0.002 mM. After hydrogel formation, the hydrogels were carefully removed, and the remaining dye solutions were analyzed using UV–Vis spectroscopy. The dye concentrations of MB (C_e) were measured in triplicate. The removal efficiencies (R) and the amount of adsorbate adsorbed at equilibrium (q_e) for MB were calculated using Eqs. 5 and 6.

3.10. Isotherm models

The isotherm equilibrium data were analyzed using two different adsorption isotherm models: Langmuir and Freundlich [51,52].

The Langmuir isotherm assumes that adsorption occurs on a homogeneous surface where each molecule has a constant enthalpy and sorption activation energy, with no interaction between the adsorbed molecules. This model simply describes the formation of a monolayer of adsorbate on the surface. The linearized Langmuir equation can be expressed as Equation 7 (Eq. 7: $1/q_e = 1/q_m + (1/q_m K_L C_e)$) where q_m (mmol/g) represents the maximum adsorption capacity and K_L is the Langmuir isotherm constant, related to the energy of adsorption (L/mg). This constant reflects the ratio between adsorption and desorption rate constants and can be associated with the Gibbs free energy (ΔG°) according to Equation 8 (Eq. 8: $\Delta G^\circ = -RT\,Ln(K_L)$, the unit of K_L being L/mol [53], T is the temperature (K) and R is the universal gas constant (J mol^{-1} K^{-1}).

The Hall parameter (R_L) was calculated using Equation 9 [35]. (Eq. 9: $R_L = 1/(1 + K_L{*}C_0)$, where C_0 is the initial concentration of the adsorbate in solution (mg/L).

Unlike its Langmuir counterpart, the Freundlich isotherm is based on the assumption that the adsorption occurs on a heterogeneous surface with interactions between adsorbed molecules. This model simply describes the formation of a multiple layers of adsorbate on heterogeneous surfaces. The logarithmic form of the Freundlich isotherm can be expressed as Equation 10 (Eq. 10: $Ln\ q_e = \ln K_F + (1/n) \ln C_e$) where K_F is the Freundlich isotherm constant ($mg^{1-(1/n)}\ L^{1/n}/g$) and n is the corresponding Freundlich constant which denotes the intensity of adsorption.

The Dubinin-Radushkevich (D-R) isotherm model is described by Equation 11 (Eq. 11: $\ln q_e = K\varepsilon^2 + \ln q_m$) where K ($mol^2/KJ^2$) is the Dubinin–Radushkevich distribution constant in mol^2 and ε is the Polanyi potential, which was calculated according to equation 12 (Eq. 12: $\varepsilon = RT\ln((C_e+1)/C_e)$) where C_e is in mol/L and R in kJ/mol K. Finally, the mean energy of sorption was assessed via Equation 13 (Eq. 13: $E = (2K)^{1/2}$ in kJ/mol). The D-R isotherm model was used to identify whether the adsorption process was chemisorption or physical adsorption.

3.11. Desorption and regeneration studies

Sixteen mg of BA and 4 mg of **NCChit-ox** were added to 1 mL of Milli-Q water in an ultrasound bath for 1 h at room temperature. Subsequently, 4 mL of a 2 % $CaCl_2$ solution were added to the dispersion and left unstirred for 24 h to allow hydrogel formation. The resulting hydrogel was transferred to 7 mL of 0.1 M HCl under stirring at 100 rpm for 1 h. It was then immersed in 5 mL of MB solutions at concentrations of 0.002 mmol/L (C_o) and stirred at 100 rpm for 3 h to complete the first adsorption/desorption cycle.

Duplicate samples were prepared for each set of adsorption/desorption experiments, and the procedure was repeated 3 times. For each cycle, the hydrogel was carefully removed from the solution and the resulting dye solution was analyzed by UV–Vis spectroscopy. The concentration of methylene blue after adsorption (C_e) was measured in triplicate. The removal efficiency (R) of MB for each cycle was calculated using Eq. 5.

3.12. Kinetic experiments

In the kinetic experiments, 20 mg of BA-based hydrogel and the **BA + NCChit-ox** - based hydrogel, as obtained in Section "hydrogel formation" were immersed into 10 mL of MB solution at a concentration of 0.02 mmol/L while varying contact time from 10 to 260 min. Samples were collected at predetermined time intervals for analyzing the residual MB concentration in the solution. The experimental data were fitted to the pseudo-first-order and pseudo-second-order kinetic models, represented by Equations 14 and 15 [54] (Eq. 14: $Ln\ (q_e - q_t) = \ln q_e - K_1 t$ and Eq. 15: $1/q_t = (1/K_2\ q_e^2) + (1/q_e)$) where q_t (mg/g) and q_e (mg/g)

correspond to the amount of MB adsorbed at time t and at equilibrium, respectively. K_1 (1 min^{-1}) and K_2 (g/mg min) are the rate constants for the pseudo-first-order and pseudo-second-order models, respectively.

3.13. Thermodynamic experiments

For the thermodynamic experiments, 20 mg of **BA** - based hydrogel and the **BA** + **NCChit-ox** - based hydrogel, as obtained in Section 2.7, were added to a MB solution at a concentration of 0.02 mmol/L. Experiments were conducted at different temperatures (298, 308, 318 and 328 K) and the final MB concentration was determined after 24 h of contact time. Enthalpy changes (ΔH°), Gibbs energy changes (ΔG°), and entropy changes (ΔS°) were evaluated using Equations 16 to 18 [26,55] (Eq. 16: $\Delta G_o = \Delta H_o - T\Delta S_o$; Eq. 17: $\Delta G_o = -RT\ Ln(\rho K_e)$ and Eq. 18: $Ln(\rho K_e) = \Delta S_o/R - \Delta H_o/(RT)$) where the distribution coefficient (K_e in L g^{-1}) was defined as the ratio of the mass of MB sorbed on 1 g of the adsorbent (q_e in mg g^{-1}) and the concentration (C_e in mg L^{-1}) of MB in the solution after reaching the equilibrium and for each temperature, is the solution density (g L^{-1}) [26].

3.14. Computational details

The starting structure for the 9-chain 10-mer chitin model was constructed using experimental crystallographic data taken from reference[56], whereas the starting structure for the 9-chain 10-mer cellulose type Iβ model was constructed using the Cellulose builder toolkit [57]. The surface acetyl-D-glucosamine units were randomly modified to match experimental conditions: 5 % were protonated and 40 % were oxidized for "pristine" chitin (**NCChit**) and **NCChit-ox**, respectively. Concerning cellulose (**NCC**), 7 % of the surface β-D-glucose units of type Iβ were sulfated. Both types of nanocrystals were described using the GLYCAM06 force field [58]. Parameters and partial charges for the modified surface units were either taken from the GLYCAM06 force field when available or computed using R.E.D. Server [59]. Methylene blue and Congo red were described using the GAFF force field [60] and their partial atomic charges were taken from references [61,62]. The substituted surface sugar units were randomly chosen; five different substituted nanocrystals were generated for each system. The crystals were introduced in truncated octahedral boxes containing TIP3P water molecules[63], ten molecules of dyes as well as counter-ions (Na^+ and/or Cl^-) for electroneutrality. While much higher than the experimental value, the corresponding dye concentration of approximately 40 mM is a fair trade-off between realism and computational limitations (polynomial increase of system sizes and sampling times at lower dye concentrations). The dye molecules were randomly placed in the bulk solvent, away from the crystal surface. The systems were minimized and equilibrated at constant volume and a temperature of 300 K, then at a constant 1 bar pressure. Production runs of 400 ns were then performed at a constant temperature of 300 K and a constant pressure of 1 bar. The temperature and pressure were respectively regulated using the velocity-rescaling (s = 2 ps) and Parrinello-Rahman (s = 5 ps, compressibility = 4.5 10^5 bar^{-1}) algorithms. The equations of motions were integrated using a 2 fs time step. Periodic boundary conditions were imposed in all dimensions of space. Short-range Coulomb and van der Waals forces were cut off at 1 nm, while long-range electrostatics were computed with the particle-mesh Ewald method. All simulations were performed and analyzed using the GROMACS 2022.4 suite [64].

4. Conclusions

In conclusion, polysaccharide-based nanocrystals and bacterial alginate (**BA**) demonstrate strong potential as effective adsorbents for the removal of methylene blue (MB) from aqueous solutions. Among the materials investigated, oxidized chitin nanocrystals (**NCChit-ox**) exhibit the highest adsorption efficiency toward MB, which can be attributed to their favorable surface charge and well-defined nanostructure. Molecular-level investigations reveal that dye removal results from a subtle balance between dye–nanocrystal interactions and dye–dye stacking, in good agreement with the experimental observations. Although BA-based hydrogels already show satisfactory performance for MB adsorption, their combination with **NCChit-ox** significantly enhances adsorption capacity. Thermodynamic and kinetic analyses confirm that the adsorption processes are spontaneous, exothermic, and mainly governed by electrostatic interactions. In addition, the hydrogels exhibit good swelling behavior and notable reusability, retaining >80 % of their adsorption performance after three cycles. Overall, these results highlight the promise of chitin-based nanomaterials and their hydrogel composites as efficient, recyclable, and sustainable adsorbents for dye removal in environmental and chemical engineering applications.

Data availability

The data supporting this article have been included as part of the Supplementary Information.

CRediT authorship contribution statement

Daniela Duarte-Serrano: Writing – original draft, Investigation. **Christophe Waterlot:** Writing – review & editing. **Christine Cézard:** Writing – review & editing, Investigation. **Benjamin Bouvier:** Writing – review & editing, Investigation. **Cesar Barrientos:** Writing – review & editing, Investigation. **Italo F. Cuneo:** Writing – review & editing. **Claudia Fuentealba:** Writing – review & editing. **Caroline Hadad:** Writing – review & editing, Writing – original draft. **Albert Nguyen Van Nhien:** Writing – review & editing, Conceptualization.

Declaration of competing interest

The authors declare that they have no known competing financial interests or personal relationships that could have appeared to influence the work reported in this paper.

Acknowledgements

This work was granted access to HPC resources of "Plateforme MatriCS" within the University of Picardie Jules Verne. "Plateforme MatriCS" is co-financed by the European Union with the European Regional Development Fund (FEDER) and the Hauts-De-France Regional Council among others. This work has benefited from the support of the National Research Agency under France 2030, MAIA Project ANR-22-EXES-0009 and of the CPER BiHauts Eco de France. C. F and A. N. V. N. would like to thank ECOS-SUD, action n °C21E01 for financial support for mobility exchange.

Supplementary materials

Supplementary material associated with this article can be found, in the online version, at doi:10.1016/j.rineng.2025.108904.

Data availability

No data was used for the research described in the article.

References

[1] N. Gaur, S. Sharma, N. Yadav, Chapter 2 - environmental pollution, in: V.K. Garg, A. Yadav, C. Mohan, S. Yadav, N. Kumari (Eds.), Green Chemistry Approaches to Environmental Sustainability, Elsevier, 2024, pp. 23–41, https://doi.org/10.1016/B978-0-443-18959-3.00010-0.

[2] N. Crini, E. Lichtfouse, G. Liu, V. Balaram, A.R.L. Ribeiro, Z. Lu, F. Stock, E. Carmona, M. Teixeira, L. Picos Corrales, J. Moreno-Piraján, L. Giraldo, C. Li, A. Pandey, D. Hocquet, G. Torri, C. grégorio, Worldwide cases of water pollution by emerging contaminants: a review, Environ. Chem Lett 20 (2022), https://doi.org/10.1007/s10311-022-01447-4.

[3] M.F.M. Mehtab Haseena, Javed Asma, Arshad Sidra, Asif Nayab, Zulfiqar Sharon, Hanif Jaweria, Water pollution and human health, Environ. Risk Assess. Remediat. 1 (3) (2017), https://doi.org/10.4066/2529-8046.100020.

[4] Solayman, A. Abd Aziz, N.Y. Yahya, K.H. Leong, L.C. Sim, M.K. Hossain, M.B. Khan, K.-D. Zoh, CQDs embed g-C3N4 photocatalyst in dye removal and hydrogen evolution: an insight review, J. Water Process Eng. 57 (2024) 104645, https://doi.org/10.1016/j.jwpe.2023.104645.

[5] K. Maheshwari, M. Agrawal, A.B. Gupta, Dye pollution in water and wastewater, in: S.S. Muthu, A. Khadir (Eds.), Novel Materials for Dye-containing Wastewater Treatment, Springer Singapore, Singapore, 2021, pp. 1–25, https://doi.org/10.1007/978-981-16-2892-4_1.

[6] L. Lin, H. Yang, X. Xu, Effects of water pollution on Human health and disease heterogeneity: a review, Front. Environ. Sci. 10 (2022), https://doi.org/10.3389/fenvs.2022.880246.

[7] M. Pooresmaeil, H. Namazi, Chapter 14 - application of polysaccharide-based hydrogels for water treatments. Hydrogels Based on Natural Polymers, Elsevier, Chen, Y., Ed, 2020, pp. 411–455, https://doi.org/10.1016/B978-0-12-816421-1.00014-8.

[8] W. Zhang, Y. Xu, X. Mu, S. Li, X. Liu, Z. Lei, Research progress of polysaccharide-based natural polymer hydrogels in water purification, Gels 9 (3) (2023) 249.

[9] F. Karchoubi, R. Afshar Ghotli, H. Pahlevani, M. Baghban Salehi, New insights into nanocomposite hydrogels; a review on recent advances in characteristics and applications, Adv. Ind. Eng. Polym. Res. 7 (1) (2024) 54–78, https://doi.org/10.1016/j.aiepr.2023.06.002.

[10] F. Clementi, Alginate production by Azotobacter vinelandii, Crit. Rev. Biotechnol. 17 (4) (1997) 327–361, https://doi.org/10.3109/07388559709146618.

[11] B.H. Rehm, S. Valla, Bacterial alginates: biosynthesis and applications, Appl. Microbiol. Biotechnol. 48 (3) (1997) 281–288, https://doi.org/10.1007/s002530051051.

[12] B.H. Rehm, Bacterial polymers: biosynthesis, modifications and applications, Nat. Rev. Microbiol. 8 (8) (2010) 578–592, https://doi.org/10.1038/nrmicro2354.

[13] C. Barrientos-Sanhueza, D. Cargnino-Cisternas, A. Díaz-Barrera, I.F. Cuneo, Bacterial alginate-based hydrogel reduces hydro-mechanical soil-related problems in agriculture facing climate change, Polym. (Basel) 14 (5) (2022) 922.

[14] V. Urtuvia, N. Maturana, F. Acevedo, C. Peña, A. Díaz-Barrera, Bacterial alginate production: an overview of its biosynthesis and potential industrial production, World J. Microbiol. Biotechnol. 33 (11) (2017) 198, https://doi.org/10.1007/s11274-017-2363-x.

[15] Q. Ding, C. Ji, T. Wang, Y. Wang, H. Yang, Hairy chitin nanocrystals: sustainable adsorbents for efficient removal of organic dyes, Int. J. Biol. Macromol. 298 (2025) 139948, https://doi.org/10.1016/j.ijbiomac.2025.139948.

[16] X. Zhang, I. Elsayed, C. Navarathna, G.T. Schueneman, E.B. Hassan, Biohybrid hydrogel and aerogel from self-assembled nanocellulose and nanochitin as a high-efficiency adsorbent for water purification, ACS Appl. Mater. Interfaces 11 (50) (2019) 46714–46725, https://doi.org/10.1021/acsami.9b15139.

[17] C. Waterlot, D. Duarte-Serrano, C. Hadad, A. Jamali, A.N. Van Nhien, Removal of Ni2+ and Cd2+ from aqueous solutions by bionanosorbents: isotherm, thermodynamic and mechanistic studies, Chemosphere 377 (2025) 144311, https://doi.org/10.1016/j.chemosphere.2025.144311.

[18] Liao, J.; Wang, Y.; Hou, B.; Zhang, J.; Huang, H., Nano-chitin reinforced agarose hydrogels: effects of nano-chitin addition and acidic gas-phase coagulation. *Carbohydr. Polym.* 2023, 313, 120902. https://doi.org/10.1016/j.carbpol.2023.120902.

[19] H. Lee, M.H. Heo, H. Jeong, S.Y. Kim, J.S. Yuk, S.H. Park, J. Shin, Water-redispersible and high-yield α-chitin nanocrystals isolated using electron-beam irradiation as adsorbents to remove heavy metals and dye, Nanoscale 15 (26) (2023) 10990–11004, https://doi.org/10.1039/D3NR00760J.

[20] T. Heinze, Cellulose: structure and properties, in: O.J. Rojas (Ed.), Cellulose Chemistry and Properties: Fibers, Nanocelluloses and Advanced Materials, Springer International Publishing: Cham, 2016, pp. 1–52, https://doi.org/10.1007/12_2015_319.

[21] B. Moussian, Chitin: structure, chemistry and biology, in: Q. Yang, T. Fukamizo (Eds.), Targeting Chitin-containing Organisms, Springer Singapore, Singapore, 2019, pp. 5–18, https://doi.org/10.1007/978-981-13-7318-3_2.

[22] N. Lin, C. Bruzzese, A. Dufresne, TEMPO-oxidized nanocellulose participating as crosslinking aid for alginate-based sponges, ACS Appl. Mater. Interfaces 4 (9) (2012) 4948–4959, https://doi.org/10.1021/am301325r.

[23] J.D. Goodrich, W.T. Winter, α-chitin nanocrystals prepared from shrimp shells and their specific surface area measurement, Biomacromolecules 8 (1) (2007) 252–257, https://doi.org/10.1021/bm0603589.

[24] Y. Fan, T. Saito, A. Isogai, Chitin nanocrystals prepared by TEMPO-mediated oxidation of alpha-chitin, Biomacromolecules 9 (1) (2008) 192–198, https://doi.org/10.1021/bm700966g.

[25] C. Ferreira Funes, A. Larach, X. Besoain, D.D. Serrano, C. Hadad, R. Pedreschi, A. N. Van Nhien, C. Fuentealba, Active coatings based on oxidized chitin nanocrystals and silk fibroins for the control of anthracnose in 'Hass' avocados, Int. J. Biol. Macromol. 253 (2023) 126673, https://doi.org/10.1016/j.ijbiomac.2023.126673.

[26] A.G.M. Shoaib, S. Ragab, A. El Sikaily, M. Yılmaz, A. El Nemr, Thermodynamic, kinetic, and isotherm studies of Direct Blue 86 dye absorption by cellulose hydrogel, Sci. Rep. 13 (1) (2023) 5910, https://doi.org/10.1038/s41598-023-33078-2.

[27] M.S. Rana, M.A. Rahim, M.P. Mosharraf, M.F.K. Tipu, J.A. Chowdhury, M. R. Haque, S. Kabir, M.S. Amran, A.A. Chowdhury, Morphological, spectroscopic and thermal analysis of cellulose nanocrystals extracted from waste jute Fiber by acid hydrolysis, Polym. (Basel) 15 (6) (2023) 1530.

[28] D. Franco, J. Piccin, E.C. Lima, G. Dotto, Interpretations about methylene blue adsorption by surface modified chitin using the statistical physics treatment, Adsorption 21 (2015), https://doi.org/10.1007/s10450-015-9699-z.

[29] S. Dhananasekaran, R. Palanivel, S. Pappu, Adsorption of Methylene Blue, Bromophenol Blue, and Coomassie Brilliant Blue by α-chitin nanoparticles, J. Adv. Res. 7 (1) (2016) 113–124, https://doi.org/10.1016/j.jare.2015.03.003.

[30] B. Farasati Far, M.R. Naimi-Jamal, M. Jahanbakhshi, S.A. Khalafvandi, M. Alian, D. Razeghi Jahromi, Decontamination of Congo red dye from aqueous solution using nanoclay/chitosan-graft-gelatin nanocomposite hydrogel, J. Mol. Liq. 395 (2024) 123839, https://doi.org/10.1016/j.molliq.2023.123839.

[31] R. Guo, L.D. Wilson, Synthetically engineered chitosan-based materials and their sorption properties with methylene blue in aqueous solution, J. Colloid Interface Sci. 388 (1) (2012) 225–234, https://doi.org/10.1016/j.jcis.2012.08.010.

[32] M. Samadi Kazemi, A. Sobhani, CuMn2O4/chitosan micro/nanocomposite: green synthesis, methylene blue removal, and study of kinetic adsorption, adsorption isotherm experiments, mechanism and adsorbent capacity, Arab. J. Chem. 16 (6) (2023) 104754, https://doi.org/10.1016/j.arabjc.2023.104754.

[33] M. Mabel, T. Sundararaman, N. Parthasarathy, J. Rajkumar, Chitin beads from Peneaus sp. Shells as a biosorbent for methylene blue dye removal, Pol. J. Environ. Stud. 28 (4) (2019).

[34] W.W. Ngah, L. Teong, M.M. Hanafiah, Adsorption of dyes and heavy metal ions by chitosan composites: a review, Carbohydr. Polym. 83 (4) (2011) 1446–1456.

[35] O. Hamdaoui, E. Naffrechoux, Modeling of adsorption isotherms of phenol and chlorophenols onto granular activated carbon: part I. Two-parameter models and equations allowing determination of thermodynamic parameters, J. Hazard. Mater 147 (1) (2007) 381–394, https://doi.org/10.1016/j.jhazmat.2007.01.021.

[36] S. Paavilainen, T. Róg, I. Vattulainen, Analysis of twisting of cellulose nanofibrils in atomistic molecular dynamics simulations, J. Phys. Chem. B 115 (14) (2011) 3747–3755, https://doi.org/10.1021/jp111459b.

[37] S.J. Hanley, J.-F. Revol, L. Godbout, D.G. Gray, Atomic force microscopy and transmission electron microscopy of cellulose from Micrasterias denticulata; evidence for a chiral helical microfibril twist, Cellulose 4 (3) (1997) 209–220, https://doi.org/10.1023/A:1018483722417.

[38] M. Ghanbari, M. Salavati-Niasari, F. Mohandes, Thermosensitive alginate–gelatin–nitrogen-doped carbon dots scaffolds as potential injectable hydrogels for cartilage tissue engineering applications, RSC Adv. 11 (30) (2021) 18423–18431, https://doi.org/10.1039/D1RA01496J.

[39] E.N. Heybet, V. Ugraskan, B. Isik, O. Yazici, Adsorption of methylene blue dye on sodium alginate/polypyrrole nanotube composites, Int. J. Biol. Macromol. 193 (2021) 88–99, https://doi.org/10.1016/j.ijbiomac.2021.10.084.

[40] G.J. Copello, A.M. Mebert, M. Raineri, M.P. Pesenti, L.E. Diaz, Removal of dyes from water using chitosan hydrogel/SiO2 and chitin hydrogel/SiO2 hybrid materials obtained by the sol-gel method, J. Hazard. Mater. 186 (1) (2011) 932–939, https://doi.org/10.1016/j.jhazmat.2010.11.097.

[41] J.A. González, J.G. Bafico, M.E. Villanueva, S.A. Giorgieri, G.J. Copello, Continuous flow adsorption of ciprofloxacin by using a nanostructured chitin/graphene oxide hybrid material, Carbohydr. Polym. 188 (2018) 213–220, https://doi.org/10.1016/j.carbpol.2018.02.021.

[42] H. Malektaj, A.D. Drozdov, J. deClaville Christiansen, Swelling of homogeneous alginate gels with multi-stimuli sensitivity, Int. J. Mol. Sci. 24 (6) (2023) 5064.

[43] P. Siqueira, É. Siqueira, A.E. de Lima, G. Siqueira, A.D. Pinzón-Garcia, A.P. Lopes, M.E.C. Segura, A. Isaac, F.V. Pereira, V.R. Botaro, Three-dimensional stable alginate-nanocellulose gels for biomedical applications: towards tunable mechanical properties and cell growing, Nanomater. (Basel) 9 (1) (2019), https://doi.org/10.3390/nano9010078.

[44] Huet, G.; Hadad, C.; González-Domínguez, J.M.; Courty, M.; Jamali, A.; Cailleu, D.; van Nhien, A.N., IL versus DES: impact on chitin pretreatment to afford high quality and highly functionalizable chitosan. *Carbohydr. Polym.* 2021, 269, 118332. 10.1016/j.carbpol.2021.118332.

[45] D. da Silva Perez, S. Montanari, M.R. Vignon, TEMPO-mediated oxidation of cellulose III, Biomacromolecules 4 (5) (2003) 1417–1425, https://doi.org/10.1021/bm034144s.

[46] C. Padilla-Córdova, B. Mongili, P. Contreras, D. Fino, T. Tommasi, A. Díaz-Barrera, Productivity and scale-up of poly(3-hydroxybutyrate) production under different oxygen transfer conditions in cultures of Azotobacter vinelandii, J. Chem. Technol. Biotechnol. 95 (11) (2020) 3034–3040, https://doi.org/10.1002/jctb.6465.

[47] A. Díaz-Barrera, N. Maturana, I. Pacheco-Leyva, I. Martínez, C. Altamirano, Different responses in the expression of alginases, alginate polymerase and acetylation genes during alginate production by Azotobacter vinelandii under oxygen-controlled conditions, J. Ind. Microbiol. Biotechnol. 44 (7) (2017) 1041–1051, https://doi.org/10.1007/s10295-017-1929-9.

[48] P. Chauhan, C. Hadad, A.H. López, S. Silvestrini, V. La Parola, E. Frison, M. Maggini, M. Prato, T. Carofiglio, A nanocellulose–dye conjugate for multi-format optical pH-sensing, Chem. Commun. 50 (67) (2014) 9493–9496, https://doi.org/10.1039/C4CC02983F.

[49] P. Chauhan, C. Hadad, A. Sartorelli, M. Zarattini, A. Herreros-López, M. Mba, M. Maggini, M. Prato, T. Carofiglio, Nanocrystalline cellulose–porphyrin hybrids: synthesis, supramolecular properties, and singlet-oxygen production, Chem. Commun. 49 (76) (2013) 8525–8527, https://doi.org/10.1039/C3CC44852E.

[50] F. Dorochesi, C. Barrientos-Sanhueza, Á. Díaz-Barrera, I.F. Cuneo, Enhancing soil resilience: bacterial alginate hydrogel vs. Algal alginate in mitigating agricultural challenges, Gels 9 (12) (2023) 988.

[51] H. Sukmana, N. Bellahsen, F. Pantoja, C. Hodur, Adsorption and coagulation in wastewater treatment – Review, Prog. Agric. Eng. Sci. 17 (1) (2021) 49–68, https://doi.org/10.1556/446.2021.00029.

[52] J. Bayuo, K. Pelig-Ba, M. Abukari, Isotherm modeling of lead (II) adsorption from aqueous solution using groundnut shell As A low-cost adsorbent, IOSR J. Appl. Chem. 11 (2018) 18–23, https://doi.org/10.9790/5736-1111011823.
[53] C. Djelloul, Experimentation, Modelisation Et Optimization De L'adsorption Des Effluents Textiles, University Mohamed Khider De Briska, 2014.
[54] J. Bayuo, M.J. Rwiza, J.W. Choi, K.M. Mtei, A. Hosseini-Bandegharaei, M. Sillanpää, Adsorption and desorption processes of toxic heavy metals, regeneration and reusability of spent adsorbents: economic and environmental sustainability approach, Adv. Colloid Interface Sci. 329 (2024) 103196, https://doi.org/10.1016/j.cis.2024.103196.
[55] G.L. Dotto, J.M.N. Santos, I.L. Rodrigues, R. Rosa, F.A. Pavan, E.C. Lima, Adsorption of Methylene Blue by ultrasonic surface modified chitin, J. Colloid Interface Sci. 446 (2015) 133–140, https://doi.org/10.1016/j.jcis.2015.01.046.
[56] P. Sikorski, R. Hori, M. Wada, Revisit of α-chitin crystal structure using high resolution X-ray diffraction data, Biomacromolecules 10 (5) (2009) 1100–1105, https://doi.org/10.1021/bm801251e.
[57] T.C.F. Gomes, M.S. Skaf, Cellulose-Builder: a toolkit for building crystalline structures of cellulose, J. Comput. Chem. 33 (14) (2012) 1338–1346, https://doi.org/10.1002/jcc.22959.
[58] K.N. Kirschner, A.B. Yongye, S.M. Tschampel, J. González-Outeiriño, C.R. Daniels, B.L. Foley, R.J. Woods, GLYCAM06: a generalizable biomolecular force field. Carbohydrates, J. Comput. Chem. 29 (4) (2008) 622–655, https://doi.org/10.1002/jcc.20820.
[59] E. Vanquelef, S. Simon, G. Marquant, E. Garcia, G. Klimerak, J.C. Delepine, P. Cieplak, F.-Y. Dupradeau, R.E.D. Server: a web service for deriving RESP and ESP charges and building force field libraries for new molecules and molecular fragments, Nucleic Acids Res. 39 (suppl_2) (2011) W511–W517, https://doi.org/10.1093/nar/gkr288.
[60] J. Wang, R.M. Wolf, J.W. Caldwell, P.A. Kollman, D.A. Case, Development and testing of a general amber force field, J. Comput. Chem. 25 (9) (2004) 1157–1174, https://doi.org/10.1002/jcc.20035.
[61] M. Enescu, J. Ridard, V. Gheorghe, B. Levy, Electron transfer modeling in condensed phase by Molecular dynamics simulation: application to methylene blue-guanine complex in water, J. Phys. Chem. B 106 (1) (2002) 176–184, https://doi.org/10.1021/jp011891f.
[62] A. Jagusiak, J. Goclon, T. Panczyk, Adsorption of Evans blue and Congo red on carbon nanotubes and its influence on the fracture parameters of defective and functionalized carbon nanotubes studied using computational methods, Appl. Surf. Sci. 539 (2021) 148236, https://doi.org/10.1016/j.apsusc.2020.148236.
[63] W.L. Jorgensen, J. Chandrasekhar, J.D. Madura, R.W. Impey, M.L. Klein, Comparison of simple potential functions for simulating liquid water, J. Chem. Phys. 79 (2) (1983) 926–935, https://doi.org/10.1063/1.445869.
[64] M.J. Abraham, T. Murtola, R. Schulz, S. Páll, J.C. Smith, B. Hess, E. Lindahl, GROMACS: high performance molecular simulations through multi-level parallelism from laptops to supercomputers, SoftwareX 1-2 (2015) 19–25, https://doi.org/10.1016/j.softx.2015.06.001.